

Article

Significantly Enhancing the Ignition/Compression/Damping Response of Monolithic Magnesium by Addition of Sm₂O₃ Nanoparticles

Milli Suchita Kujur^{1,2}, Ashis Mallick¹, Vyasaraj Manakari² , Gururaj Parande² ,
Khin Sandar Tun² and Manoj Gupta^{2,*}

¹ Department of Mechanical Engineering, Indian Institute of Technology (ISM), Dhanbad, Jharkhand 826004, India; millisuchitakujur@gmail.com (M.S.K.); mal123_us@yahoo.com (A.M.)

² Department of Mechanical Engineering, National University of Singapore, 9 Engineering Drive 1, Singapore 117576, Singapore; mbvyasaraj@u.nus.edu (V.M.); gururaj.parande@u.nus.edu (G.P.); mpekhst@nus.edu.sg (K.S.T.)

* Correspondence: mpegm@nus.edu.sg; Tel.: +65-6516-6358

Received: 7 July 2017; Accepted: 6 September 2017; Published: 9 September 2017

Abstract: The present study reports the development of Mg–Sm₂O₃ nanocomposites as light-weight materials for weight critical applications targeted to reduce CO₂ emissions, particularly in the transportation sector. Mg-0.5, 1.0, and 1.5 vol % Sm₂O₃ nanocomposites are synthesized using a powder metallurgy method incorporating hybrid microwave sintering and hot extrusion. The microstructural studies showed dispersed Sm₂O₃ nanoparticles (NPs), refinement of grain size due to the presence of Sm₂O₃ NPs, and presence of limited porosity. Microhardness and dimensional stability of pure Mg increased with the progressive addition of Sm₂O₃ NPs. The addition of 1.5 vol % of Sm₂O₃ NPs to the Mg matrix enhanced the ignition temperature by ~69 °C. The ability of pure Mg to absorb vibration also progressively enhanced with the addition of Sm₂O₃ NPs. The room temperature compressive strengths (CYS and UCS) of Mg–Sm₂O₃ nanocomposites were found to be higher without having any adverse effect on ductility, leading to a significant increase in energy absorbed prior to compressive failure. Further, microstructural characteristics are correlated with the enhancement of various properties exhibited by nanocomposites.

Keywords: Magnesium; Sm₂O₃ nanoparticles; compression properties; damping; microstructure; ignition

1. Introduction

Magnesium (Mg) is the lightest structural metal and the third most abundant element in the Earth's hydrosphere and sixth most abundant in the Earth's crust, making it readily available [1]. Mg has a density of 1.74 g/cc which is ~35.56%, ~61.39%, and ~77.89% lower than that of aluminium (2.7 g/cc), titanium (4.506 g/cc), and iron (7.87 g/cc), respectively [2]. In addition to this, Mg exhibits good mechanical and thermal properties, damping capacity, excellent castability, and machinability [3]. Mg-based materials have always been used in various industrial sectors such as aerospace, energy, construction, automotive, security, and defense, all of which are crucial to the sustainability and growth of the global economy. Increased demand for light-weighting drives the interest in Mg-based materials to be used in above-mentioned sectors striving for weight reduction, higher fuel efficiency, and payload capacity leading to reduced CO₂ emissions. However, one of the major challenges is the necessity to reduce environmental impact both in their production, end-use, and recyclability. Adoption of fabrication techniques with reduced processing time and cost such as hybrid microwave

sintering adopted in this study can result in significant energy savings which is economically viable for industries and environmentally friendly in the reduction of CO₂ emissions [4].

Currently, Mg is also finding application in biomedical engineering owing to its superior biocompatibility [5]. Mg, being an important electrolyte for human metabolism, is the fourth most abundant cation present in the body and is a cofactor in more than 300 enzyme systems that help in regulating diverse biochemical reactions in the body [6]. Overall, 99% of total Mg present in our body is in bone, muscles, and soft-muscular tissues [7]. Mg exhibits elastic modulus (41–45 GPa) closer to that of human bone (3–20 GPa) in comparison to other materials such as titanium (100–110 GPa) and stainless steel (189–205 GPa) showing, in addition, no indication of local or systemic toxicity and hence is therefore being encouraged as a biomaterial by the scientific community [8]. It is biocompatible as well as biodegradable [9] which further helps in eliminating corrective surgery and patient trauma. However, its extensive use is limited owing to its limited room temperature ductility, creep, corrosion resistance, and performance at elevated temperature [2]. Hence, researchers are actively investigating Mg-based nanocomposites as lightweight structural materials having low density, high strength, stiffness, and durability with improved corrosion resistance and acceptable performance at elevated temperatures [10]. Nanocomposites form an emerging class of materials with extremely good mechanical properties coupled with thermal integrity [11] owing to the presence of dimensionally stable ceramic or metallic reinforcements, which provide high mechanical strength as well as ductility [4].

As per the literature, Mg and its alloys have already been successfully incorporated with ceramic oxide nanoparticles (NPs) such as ZnO, Al₂O₃, ZrO₂, TiO₂, and Y₂O₃ and characterized for various mechanical properties [3]. Results obtained so far are promising, warranting further exploration of new systems. Rare earth elements (REEs) have been recently used to alloy pure Mg with encouraging results [12–17]. Rare earth oxides are natural choices as the addition of rare earth elements (REEs) as alloying elements enhances various properties of magnesium. However rare earth elements are toxic in nature and the use of rare earth oxides in nano-length scale is a viable option as they can be used in lower amounts to realize the improvement in properties (typically less than 2% by volume). There are seventeen rare earth oxides (REOs) and they have similar chemical properties by nature [6]. REOs, owing to their strong rare-earth–oxygen interactions have been reported to significantly reduce the grain size which leads to an increase in strength owing to a refined microstructure [18]. Further, they help in gathering of segregated solute impurities at the grain boundaries, alleviating the concentration of such deleterious solutes in the lattice and leading to improved ductility [19]. Hence, the addition of REOs may help in realizing a good strength-ductility combination. Also, incorporation of REOs at the nanoscale and spreading them into the interior of the grains encourages dislocation trapping by the REO particles in the interior of the grains, helping sustain work hardening and resulting in uniform elongation [19]. For example, Mg has been incorporated with yttrium oxide NPs and the tensile properties improved both at room and elevated temperature [11]. However, the main concern that arises with the use of REOs as a part of biomedical applications is their relatively unknown effects on the physiological system and research needs to be carried out if these oxides are too toxic for use as biomaterials [20].

Sm₂O₃ is one such REO having density 8.347 g/cc with high hardness Vickers (438 HV), high melting temperature (2335 °C), elastic modulus (183 GPa), Gibbs free energy (−1734.9 KJ·Mol^{−1}) [21,22]. Sm₂O₃ is an important rare earth oxide and its current scope lies in the field of solar cells, semiconductor gas, biochemical sensors, laser and photonic devices, precision guided weapons, and is also an active catalyst for CO hydrogenation [23]. Sm₂O₃ is also used as a bone-seeking radiopharmaceutical providing therapeutic irradiation to osteoblastic bone metastases [24]. The in-vitro analysis of Sm₂O₃ was found to be excellent with an appropriate cell response for a bone-contacting material and could support the initial stages of osteogenesis [24]. The response of osteoblast-like cells to Sm₂O₃ assure the non-cytotoxicity of the material and biofunctionality making it potentially useful in the field of biomaterials [24].

Also, with the ban on Mg being lifted by Federal Aviation Administration (FAA) in 2015, there is a renewed interest in replacing Al alloy based materials in the aircraft seat components, and until now, Elektron[®]WE43, Elektron[®]21 and Elektron[®]675 alloys have complied with new FAA regulations [25]. Incorporation of rare earth elements have resulted in a better ignition performance of Mg wherein Mg-10.6Y alloy and Mg3.5Y0.8Ca alloys have reported no ignition until ~1000 °C [16]. Although the research on the ignition resistance of Mg-based nanocomposites is still in its early stages, promising results for Mg-alloys can be of great encouragement to develop materials with superior overall properties. Accordingly, in the present work, the microstructural, ignition, compression, and damping properties are analyzed for the addition of 0.5, 1.0, and 1.5 vol % of Sm₂O₃ NPs in pure Mg.

2. Materials and Methods

2.1. Materials

The choice of material for metal matrix and reinforcement was Mg and Sm₂O₃, respectively. Magnesium powder of 98.5% purity with a size range of 60–300 μm was supplied by Merck, Germany. Sm₂O₃ powder with a size range of 20–30 nm was supplied by US Research Nanomaterials, Inc., Houston, TX, USA.

2.2. Synthesis

Powder Metallurgy technique assisted by hybrid microwave sintering was used for synthesis of pure Mg and (0.5, 1 and 1.5 vol %) Sm₂O₃ nanocomposites. Blending was done for the carefully weighed samples of pure Mg powder and Sm₂O₃ NPs in a RETSCH PM-400 mechanical alloying machine (Haan, Germany). Cold compaction was done post-blending at a uniaxial pressure of 1000 psi. The obtained billets (35-mm diameter and 40-mm height) were sintered using a hybrid microwave sintering technique at 630 °C in a 2.45 GHz, 900 W Sharp microwave oven. The benefits of hybrid microwave sintering over conventional sintering has been previously reported [10]. The billets were soaked at 450 °C for 2 h prior to extrusion. A 150 T hydraulic press was used to extrude the billets at a die temperature of 400 °C at an extrusion ratio of 20.25:1 to get cylindrical rods of 8 mm diameter. The extruded samples were characterized for microstructural, physical, and mechanical properties.

2.3. Microstructural Characterization

The metallographic polished samples in the extruded state were studied to investigate the grain size, reinforcement distribution, and interfacial integrity between the Mg matrix and Sm₂O₃ reinforcement. The OLYMPUS metallographic microscope (Leica Microsystems (SEA) Pte Ltd., Singapore, Singapore) and JEOL JSM-5800 LV Scanning Electron Microscope (SEM) coupled with Energy Dispersive Spectroscopy (EDS) (Jeol USA Inc., Peabody, MA, USA) were used for the microstructural characterization studies. The grain size was estimated by using a mathematical code developed in-house.

2.4. Physical Properties

2.4.1. Density Measurement

The density of three polished extruded samples for each composition was measured using the Archimedes principle. An A&D HM-202 electronic balance (Bradford, MA, USA) with an accuracy of 0.0001 g was used for measuring accurately the weights of the polished samples separately both in air and when immersed in distilled water. The theoretical densities of the samples were calculated assuming they are dense and there is no Mg–Sm₂O₃ interfacial reaction. The volume percentage of porosity in each case was computed using the theoretical and experimental density values.

2.4.2. Microhardness

Flat and polished specimens were used for micro hardness testing. A Shimadzu HMV automatic digital micro hardness tester (Kyoto, Japan) with a Vickers indenter with a phase angle of 136° was utilized for this purpose. The samples were subjected to a micro indentation load of 245 gf for a dwell time of 15 s. The tests were performed as per ASTM E384-16 standard. 15 readings were taken for each sample to ensure repeatability and accuracy of the results.

2.4.3. Coefficient of Thermal Expansion (CTE)

The CTE values of pure Mg and Mg–Sm₂O₃ nanocomposites were analyzed using a LINSEIS TMA PT 1000LT thermo-mechanical analyzer (Tokyo, Japan). The argon flow was maintained at 0.1 litres per min (lpm) while heating rate was set at 5 °C/min. The displacement of the samples was measured using an alumina probe in a temperature range of 50–400 °C. Three samples were tested to check the response.

2.4.4. Ignition Temperature

The ignition temperature of the extruded pure Mg and Mg–Sm₂O₃ nanocomposite samples (2 mm × 2 mm × 1 mm) was determined using a Shimadzu DTG-60H Thermo Gravimetric Analyser (Kyoto, Japan). The samples were heated from 30 to 750 °C at a heating rate of 10 °C/min in purified air with a flow rate of 50 mL/min. Three samples were tested to check the response.

2.5. Mechanical Properties

2.5.1. Compression Testing and Fracture Behavior

The compressive properties of the extruded pure Mg and Mg–Sm₂O₃ nanocomposite samples were determined in accordance with ASTM test method E9-09 using an MTS-810 testing machine (Eden Prairie, MN, USA) with a strain rate set at $8.334 \times 10^{-5} \text{ s}^{-1}$ on test specimens of 8 mm diameter and 8 mm length. Five samples were tested for each composition to ensure the repeatability of the test. Fractography was done for the compressive fractured samples using JEOL JSM-5800 LV Scanning Electron Microscope (SEM) to get a better understanding of the possible modes of the failure.

2.5.2. Elastic Modulus and Damping Behavior

A damping analyzer (IMCE, Genk, Belgium) was used for analyzing the elastic modulus and damping response of pure Mg and Mg–Sm₂O₃ nanocomposites using a resonant frequency as per ASTM E1876-09. Two samples were used for the analysis were of 60 mm in length and 8 mm in diameter.

3. Results and Discussion

3.1. Microstructural Characterization

The grain size measurements for pure Mg and the nanocomposite samples are shown in Table 1. The size of the grains for pure Mg was found to decrease with the increasing presence of Sm₂O₃ NPs. Mg-0.5 vol % Sm₂O₃, Mg-1.0 vol % Sm₂O₃, Mg-1.5 vol % Sm₂O₃ exhibited grain size of 21.4 μm, 17.6 μm, and 12.9 μm which is ~16.73%, ~31.51%, and ~49.80% lower than that of pure Mg (25.7 μm), respectively. The reduction in grain size for the nanocomposite can be attributed to the grain boundary pinning mechanism where the Sm₂O₃ NPs pinned the recrystallized grains of Mg, hence restraining its growth, and not to particle stimulated nucleation [26]. Dispersed Sm₂O₃ NPs within the Mg matrix can be seen in Figure 1a–c. This can be attributed to the proper selection of blending, compaction, and sintering parameters. Further, it can also be stated that the extrusion process having high extrusion ratio (20.25:1) is able to break the agglomeration and disperse the NPs uniformly as can be seen in Figure 1. However, some agglomerated sites may still be present after the extrusion process. This dispersed

Sm₂O₃ NPs promotes more uniform heating through microwaves and demonstrates the effectiveness of using hybrid microwave sintering for the synthesis of Mg-Sm₂O₃ nanocomposites.

Table 1. Results of microstructure, coefficient of thermal expansion (CTE), and microhardness studies.

Material	Grain Size (μm)	Aspect Ratio	Hardness (Hv)	CTE ($\times 10^{-6}/\text{K}$)
Pure Mg	25.7 ± 2.6	1.39 ± 0.41	54 ± 2	26.27
Mg-0.5 Sm ₂ O ₃	21.4 ± 2.3 (↓16.73%)	1.36 ± 0.20	64 ± 3 (↑18.52%)	25.82 (↓1.71%)
Mg-1.0 Sm ₂ O ₃	17.6 ± 1.8 (↓31.51%)	1.33 ± 0.16	71 ± 2 (↑31.48%)	24.99 (↓4.87%)
Mg-1.5 Sm ₂ O ₃	12.9 ± 2.2 (↓49.80%)	1.52 ± 0.30	73 ± 1 (↑35.18%)	24.11 (↓8.22%)

(↑x%) and (↓x%) indicates the percentage increase and decrease in the property with respect to pure Mg by x%, respectively.

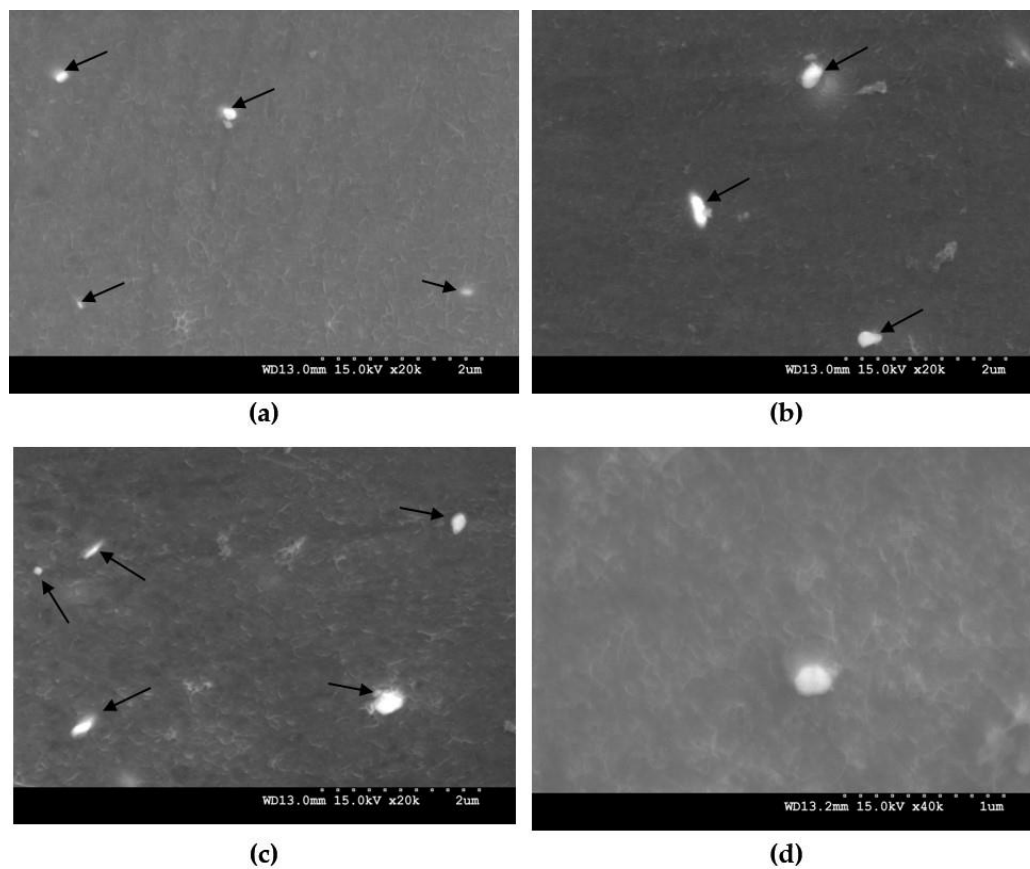


Figure 1. Scanning electron microscopy (SEM) images showing the distribution of Sm₂O₃ nanoparticles (indicated by the arrows) in Mg-Sm₂O₃ nanocomposites: (a) Mg-0.5 vol % Sm₂O₃ (b) Mg-1 vol % Sm₂O₃ (c) Mg-1.5 vol % Sm₂O₃ (d) interfacial integrity of Mg-1.0 vol % Sm₂O₃ nanocomposite.

3.2. Physical Properties

3.2.1. Density

The theoretical and experimental densities of the pure Mg and Mg-Sm₂O₃ nanocomposite samples are shown in Table 2. The experimental density of the nanocomposite samples was found to be increasing with the progressive addition of Sm₂O₃ NPs and can be attributed to the difference in density between Sm₂O₃ NPs (8.34 g/cc) and pure Mg (1.74 g/cc). As seen from Table 2, the porosity values are also found to be increasing with increasing density and the Mg-1.5 vol % Sm₂O₃ nanocomposite exhibited highest porosity value. The low wettability, agglomeration rate, and pore nucleation at the Mg-Sm₂O₃ interface could be the main reasons behind the increase in porosity with the increase

in vol % of Sm₂O₃ NPs in Mg [27]. Further, no observed macrostructural defects were observed on sintered samples and extruded rods, demonstrating the efficiency of hybrid microwave sintering and hot extrusion to synthesize near-dense magnesium-based nanocomposites [28].

Table 2. Density measurements of pure magnesium and Mg-Sm₂O₃ nanocomposites.

Material	Theoretical Density (g/cc)	Experimental Density (g/cc)	Porosity (%)
Pure Mg	1.74	1.7265 ± 0.0142	0.78
Mg-0.5 Sm ₂ O ₃	1.773	1.7287 ± 0.0147	2.50
Mg-1.0 Sm ₂ O ₃	1.806	1.7531 ± 0.0047	2.92
Mg-1.5 Sm ₂ O ₃	1.839	1.7838 ± 0.0085	3.00

3.2.2. Microhardness

The microhardness measurements for pure Mg and the nanocomposite samples are shown in Table 1. The progressive addition of Sm₂O₃ NPs resulted in a steady increase in the hardness values of pure Mg. With the addition of 1.5 vol % Sm₂O₃, a maximum average value of 73 Hv was observed which is ~35.18% greater than that of pure Mg (54 Hv). The presence of high hardness Sm₂O₃ NPs (430 Hv), reduced grain size, and constraint to localized deformation during indentation due to the presence of harder Sm₂O₃ NPs are the main inferences for the increase in the microhardness of the nanocomposite samples.

3.2.3. Coefficient of Thermal Expansion (CTE)

The coefficient of thermal expansion values for pure Mg and Mg-Sm₂O₃ nanocomposites samples are shown in Table 1. The CTE values for Mg-0.5 vol % Sm₂O₃ ($25.82 \times 10^{-6}/\text{K}$), Mg-1.0 vol % Sm₂O₃ ($24.99 \times 10^{-6}/\text{K}$), and Mg-1.5 vol % Sm₂O₃ ($24.11 \times 10^{-6}/\text{K}$) were found to be ~1.71%, ~4.87, and ~8.22% lower than that of pure Mg ($26.27 \times 10^{-6}/\text{K}$). The CTE values of pure Mg follows a linear decreasing trend with the increasing addition of Sm₂O₃ NPs, which is found to be in accordance with the theory that the thermal expansion of composites is governed by the competing interactions of expansion of the Mg matrix and the constraint of reinforcement particles through their interfaces. This behavior can be attributed to the lower CTE value of Sm₂O₃ ($8.5 \times 10^{-6}/\text{K}$) reinforcement as compared to that of pure Mg ($26.27 \times 10^{-6}/\text{K}$) and the presence of ceramic reinforcements in the matrix, hence maintaining the dimensional stability of pure Mg.

For comparison purposes, theoretical CTE values of Mg-Sm₂O₃ nanocomposites were determined by using the Rule of Mixture (ROM) model [29], which is expressed as:

$$\alpha_c = \alpha_m \cdot v_m + \alpha_p \cdot v_p \quad (1)$$

where α is the CTE, $10^{-6}/\text{K}$; v is the volume fraction and subscripts c , m , p refers to the composite, matrix, and reinforcement phase, respectively. It was observed that the experimental values of CTE obtained were lower than the theoretical values of 27.1, ~27.01, ~26.91, and $\sim 26.82 \times 10^{-6}/\text{K}$ for pure Mg, Mg-0.5 vol % Sm₂O₃, Mg-1 vol % Sm₂O₃, and Mg-1.5 vol % Sm₂O₃, respectively. This can be attributed to the overriding effect of presence and increasing amount of Sm₂O₃ over that of increasing level of porosity of Mg-Sm₂O₃ nanocomposites (Table 2).

3.2.4. Ignition Properties

The onset of ignition occurs only when the stable surface oxide of Mg-based materials tends to lose its protective properties [30]. Pure Mg can auto-ignite in solid state during heating due to the rapid increase in localized heat that causes melting and evaporation of the metal locally. When the Mg vapor is in contact with air at the gas/metal interface, the metal ignites. However, with the modification of the chemistry of the material by the addition of thermally stable alloying elements and reinforcements, the mechanism changes and can delay the onset of ignition [16]. Therefore, an attempt has been made

to study and analyze the effect of thermally stable rare earth oxides (Sm_2O_3 in the current system) on the ignition temperature of monolithic magnesium.

The ignition results using thermogravimetric analysis (TGA) are presented in Table 3. The ignition point is 610 and 613 °C for 0.5 and 1.0 vol % Sm_2O_3 and then escalates to 650 °C for 1.5 vol % of Sm_2O_3 which is ~69 °C more than pure Mg (581 °C). The ignition temperature for 1.5 vol % of Sm_2O_3 is found to be higher than most of the commercially available magnesium alloys such as AZ31, AZ61, AZ63, AZ91, AM50, AM60, ZK40A, ZK51A, and ZK60A [16] (Table 3). The ascending behavior of the point of ignition and the enhanced resistance to ignition with increasing volume fraction of Sm_2O_3 NPs may be attributed to the lower CTE values, thus maintaining the thermal and dimensional stability of the nanocomposites [26]. In addition, the presence of Sm_2O_3 NPs in the Mg matrix assists in reducing specific areas of oxidation and hence assists in delaying the onset of ignition in the Mg- Sm_2O_3 nanocomposites. It has been previously reported that Sm_2O_3 is a stable protective oxide in air at temperatures up to at least 593 °C [31]. Further, the molecular volume of oxide (ϑ^a) is 1.21 for Sm_2O_3 and both its oxidation states (+2 and +3) form stable protective oxides [32]. Since Sm_2O_3 has a high affinity to oxygen owing to strong rare-earth–oxygen interactions, a protective barrier layer is formed on the surface of Mg, restraining its reaction with oxygen. The results in Table 3 indicated that 1.5 vol % of Sm_2O_3 is most effective and the variation in ignition temperature between 0.5 and 1 vol % Sm_2O_3 was negligible, suggesting the requirement of a certain critical threshold of Sm_2O_3 to significantly enhance the ignition temperature. Further work is continuing in this area.

Table 3. Results of ignition temperatures characterization.

Material	Ignition Temperature (°C)	Thermal Conductivity (W/m·K)
Pure Mg	581	135
Mg-0.5 Sm_2O_3	610	134.32
Mg-1.0 Sm_2O_3	613	133.65
Mg-1.5 Sm_2O_3	650	132.97
AZ31	628	
AZ61	559	
AZ63	573	
AZ91	600	
AM50	585	-
AM60	525	
ZK40A	500	
ZK51A	552	
ZK60A	499	

The ignition temperature values of commercially available magnesium alloys such as AZ31, AZ61, AZ63, AZ91, AM50, AM60, ZK40A, ZK51A, and ZK60A are compiled from references given in [16].

The thermal conductivity (W/m·K) at 400 °C calculated theoretically by rule of mixtures and ignition temperature can be correlated for the Mg- Sm_2O_3 nanocomposites to understand the ignition behavior [26]. The ignition temperature ascends with the decrease in thermal conductivity with the increasing content in the volume fraction of Sm_2O_3 , as seen from Table 3. It can be inferred that the addition of Sm_2O_3 NPs helped in increasing the insulating property of pure Mg [33]. Further, the thermal conductivity of the composites is directly related to the amount of reinforcement added to the matrix, and in view of the ability of reinforcement to reduce the availability of metallic matrix for ignition, also leads to increased ignition performance with progressive addition of Sm_2O_3 NPs [34].

However, the underlying dominating mechanisms determining the ignition temperatures of Mg-based materials are complex and are not very well known, especially of the nanocomposites. Therefore, further study on the mechanisms of increase/decrease in the ignition temperature with the presence of Sm_2O_3 NPs and the dependence of the ignition characteristics on the size of the NPs will be an interesting direction of research.

3.3. Mechanical Properties

3.2.5. Compression Properties and Fracture Behavior

The room temperature compressive properties and their stress–strain relationship is shown in Table 4 and Figure 2, respectively. As it can be seen from Table 4, the compressive yield strength (0.2 CYS) of Mg increased from 74 to 87 MPa, 118, and 128 MPa with the addition of 0.5, 1.0, and 1.5 vol % of Sm_2O_3 NPs, respectively. The ultimate compressive strength (UCS) values for the Mg– Sm_2O_3 nanocomposites also increased with the progressive addition of Sm_2O_3 NPs with Mg-1.5 vol % Sm_2O_3 exhibiting the maximum UCS of 395 MPa, which is ~58.63% greater than pure Mg. The compressive fracture strain values of Mg– Sm_2O_3 nanocomposites also increased up to 1 vol % addition of Sm_2O_3 NPs, and maximum fracture strain was exhibited by Mg-1 vol % Sm_2O_3 with 20.1% (~15.51% greater than pure Mg). With the further addition of Sm_2O_3 NPs (1.5 vol %), a decrease in fracture strain value of 17.2% was observed. This reduction in fracture strain for Mg-1.5 vol % Sm_2O_3 (~1.14% lesser than pure Mg) is very marginal and the addition of Sm_2O_3 NPs helps in maintaining the ductility while increasing the strengths significantly. The increase in the 0.2 CYS and UCS of Mg– Sm_2O_3 nanocomposites can be attributed to (a) presence of fairly dispersed, hard Sm_2O_3 NPs [35]; (b) significant grain refinement (Table 1) [33]; (c) effective transfer of load from the Mg matrix to Sm_2O_3 NPs [36]; (d) mismatch of the elastic modulus and coefficient of thermal expansion values leading to generation of dislocations [37], and (e) Orowan strengthening due to the presence of Sm_2O_3 NPs [37]. The energy absorption (EA) during the process of compressive loading until failure also increased with the progressive addition of Sm_2O_3 NPs. Mg-1 vol % Sm_2O_3 nanocomposite exhibited the maximum EA value of 42.9 MJ/m³ which is ~60.07% greater than that of pure Mg. The enhanced EA of the nanocomposites with respect to pure Mg shows its potential to be used in damage tolerant designs.

Table 4. Results of room temperature compression testing.

Material	0.2 CYS (MPa)	UCS (MPa)	Fracture Strain (%)	Energy Absorbed (MJ/m ³)
Pure Mg	74 ± 3	249 ± 6	17.4 ± 0.3	26.8 ± 0.7
Mg-0.5 Sm_2O_3	87 ± 1 (↑17.56%)	285 ± 6 (↑14.45%)	19.8 ± 0.6 (↑13.79%)	33.0 ± 1.3 (↑23.13%)
Mg-1.0 Sm_2O_3	118 ± 2 (↑59.45%)	331 ± 7 (↑32.93%)	20.1 ± 0.7 (↑15.51%)	42.9 ± 2.9 (↑60.07%)
Mg-1.5 Sm_2O_3	128 ± 5 (↑72.97%)	395 ± 7 (↑58.63%)	17.2 ± 0.5 (↓1.14%)	41.2 ± 2.4 (↑53.73%)

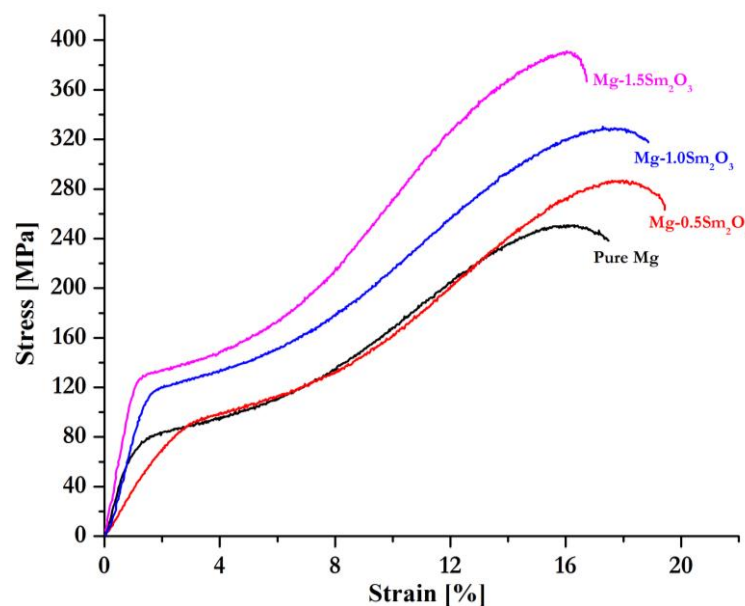


Figure 2. Stress–strain curves of pure Mg and the synthesized Mg– Sm_2O_3 nanocomposites during compression loading.

Under compression along the extrusion direction of Mg based materials, deformation occurs by twin, followed by slip [38]. The upward concave (sigmoidal) nature of compressive flow curves (Figure 2) with high work hardening further affirms that the compressive deformation occurs by a twinning process. Though the grain refinement is believed to suppress both twin and slip [39], in turn enhancing the strength of nanocomposites, this effect comes at the expense of compressive ductility. Conversely, the results show that compressive failure strain of the developed Mg-Sm₂O₃ nanocomposites were superior when compared to pure Mg upto 1 vol % addition of Sm₂O₃ NPs and was comparable to pure Mg for Mg-1.5 vol % Sm₂O₃. This can be explained by the fact that, in addition to the role of grain size on the activation energy of twinning, texture also influences the deformation twinning. Additions of rare earth oxides, such as Sm₂O₃, can facilitate grain alignment, favoring both slip and deformation twinning [40]. Thus, the presence of Sm₂O₃ NPs would help in delaying the twinning by activation of additional competing slip/twin deformation modes by the change in crystallographic orientation, thereby contributing to increased failure strain. Further studies, such as electron back-scattered diffraction (EBSD), are required to confirm the evolution of crystallographic texture in pure Mg due to incorporation of Sm₂O₃ NPs. To confirm the mode of failure under compression, fracture studies were performed. Under compressive loading, fracture surfaces are at about 45 degrees with respect to the compression testing direction. Shear bands were observed (see Figure 3), which is an indication of shear mode of failure.

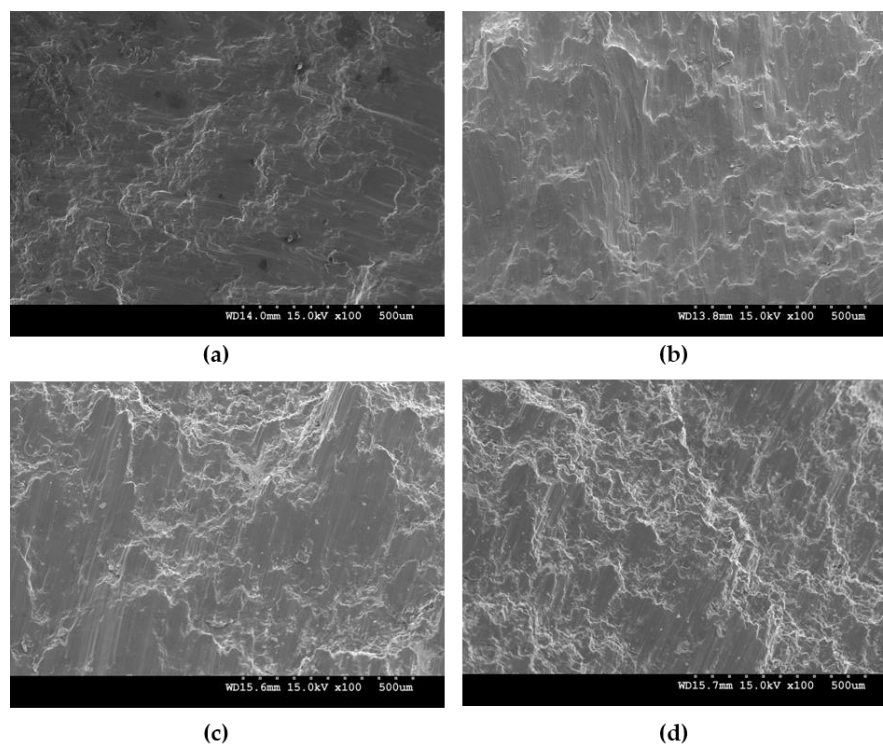


Figure 3. Fractographs after compressive loading of: (a) Pure Mg; (b) Mg-0.5 vol % Sm₂O₃; (c) Mg-1 vol % Sm₂O₃, and (d) Mg-1.5 vol % Sm₂O₃.

Figure 4 provides an overview of the improvements observed in UCS and fracture strain by the addition of Sm₂O₃ NPs to pure Mg in comparison to other ceramic, hybrid (ceramic + metallic), and amorphous reinforcements synthesized by powder metallurgy. It can be seen from Figure 4 that, Mg-Sm₂O₃ nanocomposites exhibited the highest UCS with better fracture strain in comparison to other ceramic reinforcements (represented by green bubble). Also, the strength values were comparable to those of hybrid (represented by blue bubble) and amorphous (represented by red bubble) particle-reinforced Mg composites. Further, it should be noted that the room

temperature compressive properties of the synthesized nanocomposites are superior or comparable to the properties of commercial magnesium alloys such as AZ91, WE43, WE54, and ME21 [1,41]. The combined enhancement in both strength-ductility properties which is better than most powder metallurgy synthesized nanocomposites justifies the use of Sm_2O_3 as a reinforcement, and would encourage researchers in the Mg community to further study its behavior and suitability for various commercial applications.

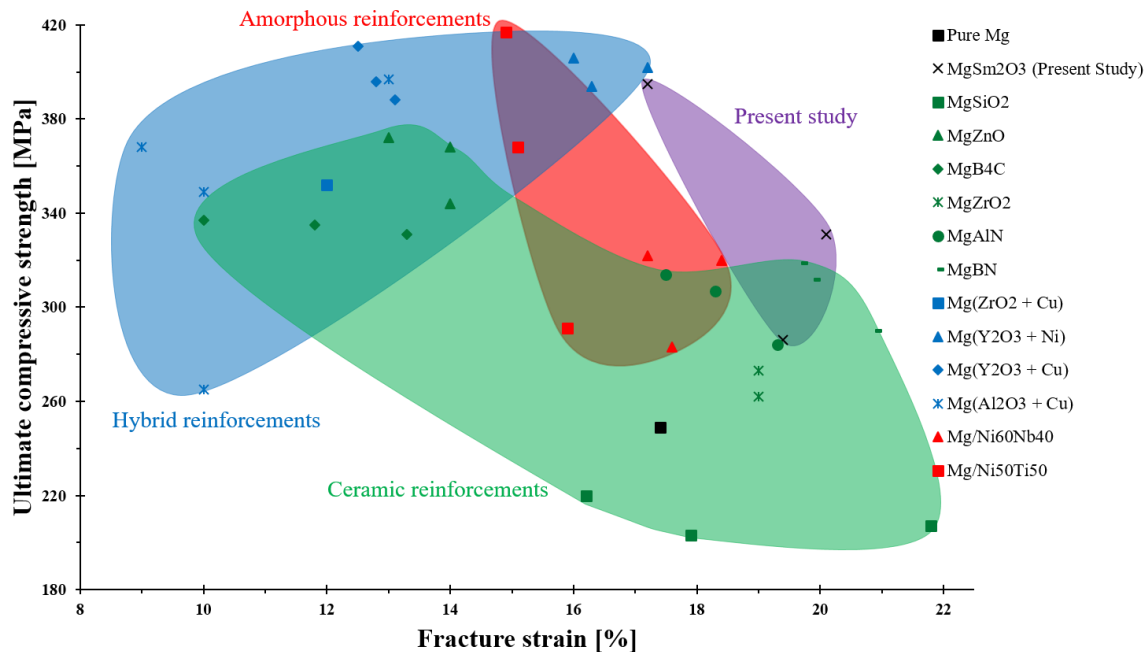


Figure 4. Bubble chart illustrating the superior compressive behaviour of Mg- Sm_2O_3 nanocomposites compiled from references [3,10].

3.2.6. Elastic Modulus and Damping Characteristics

Figure 5 shows a set of amplitude–time plots of representative samples and Table 5 lists damping loss rate, damping capacity, and elastic moduli of pure Mg and their nanocomposite samples. The vibration signal from each sample is recorded in terms of amplitude vs. time in free vibration mode. The results clearly indicate that the amplitude and time taken to stop the vibration are different for each material and the addition of Sm_2O_3 NPs significantly enhances the damping characteristics of pure Mg. It can be seen from Figure 5 that the amplitude decreases gradually for pure Mg as against steeper fall in Mg- Sm_2O_3 nanocomposites. With the addition of 0.5 and 1 vol % Sm_2O_3 in Mg matrix, the time taken to damp the vibrations is reduced significantly from 0.65 to 0.37 and 0.29 s, respectively. Most of the vibrations are ceased in less than ~ 0.2 s with the addition of 1.5 vol % Sm_2O_3 .

Table 5. Elastic modulus and damping characteristics of Mg- Sm_2O_3 nanocomposites.

Material	Damping Loss Rate	Damping Capacity	Elastic Modulus (GPa)
Pure Mg	8.2 ± 0.2	0.000394 ± 0.000021	42.3 ± 0.14
Mg-0.5 Sm_2O_3	20.2 ± 0.4 (* 2.46)	0.000719 ± 0.000017 ($\uparrow 82.48\%$)	43.7 ± 0.1 ($\uparrow 3.30\%$)
Mg-1 Sm_2O_3	29.35 ± 1.2 (* 3.57)	0.001049 ± 0.00058 ($\uparrow 166.24\%$)	45.4 ± 0.08 ($\uparrow 7.32\%$)
Mg-1.5 Sm_2O_3	36.65 ± 0.9 (* 4.47)	0.0011395 ± 0.0008 ($\uparrow 189.21\%$)	44.9 ± 0.2 ($\uparrow 6.14\%$)

(* x) indicates the increase in the property with respect to pure Mg by x times; ($\uparrow x\%$) and ($\downarrow x\%$) indicates the percentage increase and decrease in the property with respect to pure Mg by x%, respectively.

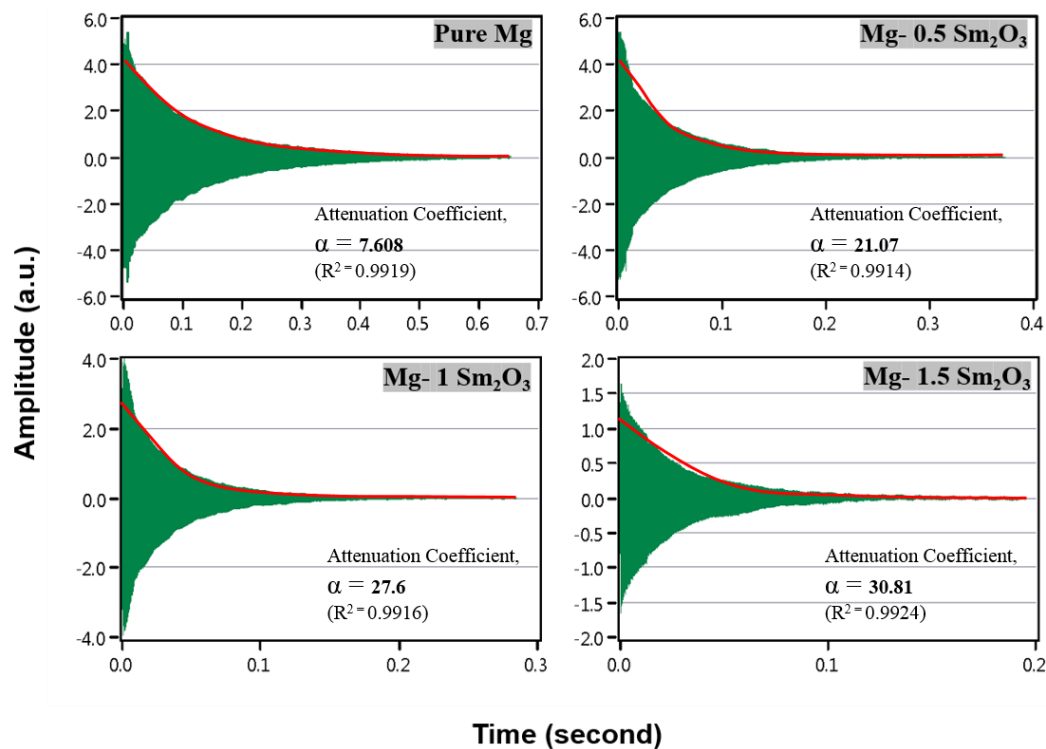


Figure 5. Damping characteristics of Mg and its nanocomposite samples.

The damping loss rate (L) which is the ability of a material to absorb vibration [42], showed an increase with the addition of Sm_2O_3 NPs (Table 5) and Mg-1.5 vol % Sm_2O_3 exhibited the maximum value of ~ 36.65 (~ 4.47 times greater than that of pure Mg). Damping loss rate as a function of volume percent of the reinforcement follows a linear fit and can be expressed using Equation (2) as,

$$L = 9.425 + 18.9 \times X \text{ (vol \%)}, (R^2 = 0.9877) \quad (2)$$

Further, the damping capacity (Q^{-1}) of Mg is also seen to be increasing with the addition of Sm_2O_3 NPs. The highest damping capacity of 0.0011395 ($\sim 189.21\%$ rise as compared to pure Mg) is shown by Mg-1.5 vol % Sm_2O_3 nanocomposite. This overall enhancement of the damping properties of Mg- Sm_2O_3 nanocomposites might be due to the presence of a plastic zone around reinforcement, increase in dislocation density, and due to other damping sources, such as grain boundary sliding mechanisms, defects, and porosities which are analyzed for their validity in the following paragraphs.

A more qualitative evaluation of damping would be by considering the attenuation coefficients. In magnesium and its alloys, the amplitude of free vibration gradually decreases with increase in time and the difference lies in the steepness of the curve which is quantified by the attenuation coefficient. In this study, the material vibrates at a resonant frequency when excited by cyclic external force and when this external force is removed, the resonant-vibration dampens gradually. Then, the amplitude of a damping vibration, $A(t)$, can be expressed as

$$A(t) = A_0 \exp\left[-\alpha t + i\frac{\pi}{f_r}t\right] \quad (3)$$

where, " t " is the time after removal of the external force, " A_0 " denotes the amplitude at $t = 0$, " α " represents the attenuation (damping) coefficient (which depends on the damping capacity of materials), and f_r denotes the resonant frequency. Here, in the case of the Mg- Sm_2O_3 nanocomposites, various vibration modes are excited, and therefore we cannot obtain the attenuation coefficient by fitting Equation (3) to the vibration-damping curve. In order to determine α in such a case, the maximum

value of positive amplitude of the damping curve has been picked up and fitted according to the following equation:

$$A(t) = A_0 e^{(-\alpha)t} + C \quad (4)$$

The amplitude and the apparent attenuation coefficients of Mg-Sm₂O₃ nanocomposites have been obtained qualitatively, where C denotes the fitting coefficient. An increasing trend in α is clearly evident from Figure 5 with the increasing amount of Sm₂O₃ NPs. A notable enhancement in the value of α from 7.608 to 30.81 is observed in case of Mg-1.5 vol % Sm₂O₃ nanocomposite as compared to pure Mg, demonstrating significant rise in damping capability.

The CTE of Sm₂O₃ and Mg is 8.5 [43] and $27.1 \times 10^{-6}/\text{K}$, respectively. This difference in thermal expansion coefficient between Mg and Sm₂O₃ might induce high residual stresses around the particulates in the Mg matrix, resulting in the formation of plastic deformation zone at the particle/matrix interface. According to the plastic zone damping model proposed by Carreno-Morelli et al. [44], the damping capacity of a material depends directly on the volume fraction of plastic zone. Therefore, progressive increase in the energy dissipation of pure Mg matrix can be attributed to the higher amount of plastic zone around Sm₂O₃ NPs and further, at higher volume fractions effects are multifold resulting in such a rise in the damping capacity of nanocomposites. Further, significantly higher damping capacities realized for Mg-1 vol % Sm₂O₃ and Mg-1.5 vol % Sm₂O₃ nanocomposites (~166.24% and 189.21% rise as compared to pure Mg, respectively) can be due to overlapping of plastic zones, caused when the plastic zone is larger compared to smaller inter-particulate distances as the volume fraction of NPs increases. This increase in the presence of plastic zones due to the presence of Sm₂O₃ NPs leading to an increase in the hardness of the nanocomposite samples (Table 1) is found to be substantially high when compared to pure Mg.

Also, thermal mismatch between the constituents leads to higher dislocation density in the matrix. The increase in dislocation density is given as follows [45],

$$\rho = \frac{9.6 \Delta\alpha\Delta T V_p}{bd} \quad (5)$$

where, " $\Delta\alpha$ " is the thermal expansion coefficient mismatch between the matrix alloy and the filler ($\times 10^{-6}/\text{K}$), " ΔT " is the difference between working and final temperatures ($^{\circ}\text{C}$), " b " is denoted by the Burger vector, " V_p " represents volume fraction (%), and " d " is the diameter of reinforcement (m). The CTE difference between Sm₂O₃ and Mg is around $18.6 \times 10^{-6}/\text{K}$. Dislocation density can be quite significant at the interface and it increases with increasing Sm₂O₃ content. For magnesium-based materials, increased dislocations are favorable for the damping enhancement as dislocation pinning contributes to the damping behavior of magnesium nanocomposites [46]. The increase in dislocation density can also be attributed to the presence of hard Sm₂O₃ NPs in the magnesium matrix [47]. In addition, the crystal structure will be distorted locally at the matrix/reinforcement interface due to the presence of two-dimensional defects at the interface. Thereby, atoms may slip up at the interface, resulting in flexible dislocation movement and leading to higher damping response [48].

Further, it has also been observed that defects play an important role in tailoring damping properties. Chung [49] suggested that defects may shift the locations during vibration, acting as internal friction resources leading to higher damping capacities. The presence of porosity further augments the damping capacity due to the heterogeneous stress-strain distribution, causing stress concentrations which results in higher dislocation movements [50]. From Table 1, an increase in the addition of Sm₂O₃ NPs increased the porosity levels of Mg-Sm₂O₃ nanocomposites. The highest damping capacity is observed for Mg-1.5 vol % Sm₂O₃ nanocomposite which has maximum matrix porosity levels as seen from Table 1. Based on the aforementioned reasons, the damping is likely to be dominated by the presence of porosity and the microstructural variations due to Sm₂O₃ NPs in Mg-Sm₂O₃ nanocomposites [35]. Elasto-thermodynamic damping and grain boundary damping are not expected to be significant in this study due to room temperature operation conditions, sample dimensions, and frequency magnitude.

Along with the compression and hardness properties, elastic modulus and damping capacity are the two important properties to investigate for applications targeting orthopedic implants. High elastic modulus (such as exhibited by steel and titanium) as compared to the natural bone results in stress-shielding effects and decreases the stimulation of new bone growth, leading to implant failure [5]. The high damping capacity of a metallic implant helps in mitigating the vibrations caused when the patient moves and suppresses the stresses developed at the bone/implant interface to achieve better osseointegration [51]. The addition of Sm_2O_3 NPs enhanced the damping characteristics of pure Mg with marginal increase in the elastic modulus (Table 5). This marginal increase in the elastic modulus with increasing amount of Sm_2O_3 NPs can be attributed to the presence of Sm_2O_3 which exhibits a higher elastic modulus of about 183 GPa [22]. However, it was observed that elastic modulus of all samples remained lower than theoretical values, which can be attributed to the presence of porosity. The effect of presence of high modulus Sm_2O_3 NPs was largely negated by the presence of relatively higher amounts of porosity in the composites.

4. Biomechanical Properties

The compressive and elastic modulus properties can be collectively termed as “biomechanical properties”. The biomechanical properties of Mg- Sm_2O_3 nanocomposites are compared with natural bone, cortical bone tissue, Ti-6Al-4V alloy, 316L stainless steel, and Co-Cr alloy in Table 6. The compressive strength is necessary for development and growth of bone and is responsible for deposition of bone material and if the compressive stress exceeds the UCS of bone it will eventually fracture. To avoid stress shielding effects, it is very important that the compressive strength of the material should not exceed the strength of the surrounding bone [52]. Natural bone exhibits certain hierarchical structures of nanometer dimensions within bone matrices and so implants are of ample concern for bone repair and regeneration in biomedical applications [53]. From the results shown in Table 6 compiled from references [8,35,54–56], the 0.2% CYS, UCS, and elastic modulus for the nanocomposite samples are closer to that of bone and bone tissues and could improve the interface between the nanocomposite and bone cells. The favored biomaterials, titanium alloys (Ti-6Al-4V), 316L stainless steel, and Co-Cr alloys exhibit significantly higher elastic modulus and are preferred only as permanent fixtures [13]. Further, in these materials there is a possibility of leaching of ions by corrosion or wear, thus decreasing their biocompatibility and causing tissue loss [57]. Also, as stated in [53], mismatch in elastic modulus of bone and steels/titanium/Co-Cr alloys is likely to result in bone resorption and loosening of implants. Hence, Mg- Sm_2O_3 nanocomposites may effectively increase the stimulation of new bone growth and re-modelling which increases the implant stability, making it favorable for applications in temporary implants avoiding stress-morbidity to the patient. The results of this study suggest that the biomechanical properties of the nanocomposites have an advantage over titanium alloys, 316L stainless steel, and Co-Cr alloys.

Table 6. Comparison between biomechanical properties of Mg- Sm_2O_3 nanocomposites with Ti-6Al-4V alloy, 316L stainless steel, Co-Cr alloy, and hard and soft tissues of the human body.

Material	Density (g/cc)	0.2% CYS (MPa)	UCS (MPa)	Fracture Strain (%)	Elastic Modulus (GPa)
Natural Bone	1.8–2.1 ^a	130–180 ^a	-	-	3–20 ^a
Cortical Bone	-	-	131–224 ^b	2–12 ^b	15–30 ^b
Ti-6Al-4V alloy	4.43 ^c	970 ^c	-	-	113.8 ^c
316L Stainless Steel	8.0 ^d	170–310 ^a	-	-	193 ^d
Co-Cr alloy	9.12–9.24 ^e	-	283–313 ^e	-	222–240 ^e
Pure Mg	1.7265	74	249	17.4	42.3
Mg-0.5 Sm_2O_3	1.7287	87	285	19.8	43.7
Mg-1 Sm_2O_3	1.7531	118	331	20.1	45.4
Mg-1.5 Sm_2O_3	1.7838	128	395	17.2	44.9

Compiled from reference: ^a—[8]; ^b—[35]; ^c—[54]; ^d—[56]; ^e—[55].

5. Conclusions

Mg-Sm₂O₃ nanocomposites were successfully synthesized using the powder metallurgy method including hybrid microwave sintering. Simultaneously, mechanical, microstructural, and damping properties were determined and analyzed. The following conclusions can be made from this study:

1. The grain size reduced with the progressive incorporation of Sm₂O₃ NPs to pure Mg, with Mg-1.5 vol % Sm₂O₃ exhibiting a maximum of 46.7% reduction in grain size with respect to pure Mg.
2. The hardness of pure Mg increased with the increasing amount of Sm₂O₃ with Mg-1.5 vol % Sm₂O₃ showing a maximum increase of ~37%.
3. The CTE values reduced with the incorporation of Sm₂O₃ NPs in pure Mg with Mg-1.5 vol % Sm₂O₃ showing a reduction of ~8.22% and the ignition temperature of Mg-1.5 vol % Sm₂O₃ showed the highest resistance to ignition (enhancement by ~69 °C), indicating superior thermal and dimensional stability.
4. The damping loss rate and damping capacity of pure Mg enhanced with the increasing amount of Sm₂O₃ NPs, with the Mg-1.5 vol % Sm₂O₃ nanocomposite displaying the best damping response (~4.5 times better than pure Mg).
5. The best compressive strength was exhibited by the Mg-1.5 vol % Sm₂O₃ nanocomposite with 0.2 CYS and UCS values increasing by ~56% and 53% when compared to pure Mg. The ductility values of Mg-Sm₂O₃ composites were either better or similar to pure Mg.
6. The superior compressive and damping properties with elastic modulus closer to natural bone makes Mg-Sm₂O₃ composites a potential choice as implant materials.

This study introduces a lightweight Mg-Sm₂O₃ nanocomposite with an excellent combination of strength, ductility, ignition resistance, and damping behavior. The superior-performance nanocomposite presented in this study has great potential in automobile and aerospace applications, and can be extended to others including defense, sport, electronic, and biomedical sectors. However, a considerable amount research is still necessary to validate these materials for their tensile, dynamic, high temperature, corrosion, fatigue, and wear properties before seeing their widespread use in industrial applications. Also, further study into the ignition mechanisms and detailed analysis is necessary to further exploit Mg nanocomposites and validate them for aerospace and defense applications. The promising results obtained in this study by the addition of rare earth oxides (REO) such as Sm₂O₃ to Mg presents a potential for the progress in research towards development of other REO-reinforced Mg nanocomposites to further ascertain the viability and the usefulness of such nanocomposites.

Author Contributions: Ashis Mallick and Manoj Gupta and Khin Sandar Tun proposed the original project and supervised the investigation. Milli Suchita Kujur performed the experiments. Milli Suchita Kujur, Vyasraj Manakari and Gururaj Parande analyzed the data, and wrote the paper with assistance from all authors. All authors contributed to the discussions in the manuscript.

Conflicts of Interest: The authors declare no conflict of interest.

References

1. Gupta, M.; Sharon, N.M.L. *Magnesium, Magnesium Alloys, and Magnesium Composites*; John Wiley & Sons: New York, NY, USA, 2011.
2. Mordike, B.; Ebert, T. Magnesium: Properties—Applications—Potential. *Mater. Sci. Eng. A* **2001**, *302*, 37–45. [[CrossRef](#)]
3. Gupta, M.; Wong, W. Magnesium-based nanocomposites: Lightweight materials of the future. *Mater. Charact.* **2015**, *105*, 30–46. [[CrossRef](#)]
4. Gupta, M.; Parande, G.; Manakari, V. An insight into high performance magnesium alloy/nano-metastable-syntactic composites. In Proceedings of the 17th Australian International Aerospace Congress: AIAC 2017, Melbourne, Australia, 26 February–2 March 2017; p. 270.

5. Manakari, V.; Parande, G.; Gupta, M. Selective laser melting of magnesium and magnesium alloy powders: A review. *Metals* **2016**, *7*, 2. [[CrossRef](#)]
6. Gröber, U.; Schmidt, J.; Kisters, K. Magnesium in prevention and therapy. *Nutrients* **2015**, *7*, 8199–8226. [[CrossRef](#)] [[PubMed](#)]
7. Classen, H.; Nowitzki, S. The clinical importance of magnesium. 2. The indications for supplementation and therapy. *Fortschr. Med.* **1990**, *108*, 198–200. [[PubMed](#)]
8. Staiger, M.P.; Pietak, A.M.; Huadmai, J.; Dias, G. Magnesium and its alloys as orthopedic biomaterials: A review. *Biomaterials* **2006**, *27*, 1728–1734. [[CrossRef](#)] [[PubMed](#)]
9. Sietsema, W. Animal models of cortical porosity. *Bone* **1995**, *17*, S297–S305. [[CrossRef](#)]
10. Sankaranarayanan, S.; Gupta, M. Review on mechanical properties of magnesium (nano) composites developed using energy efficient microwaves. *Powder Metall.* **2015**, *58*, 183–192. [[CrossRef](#)]
11. Ubaid, F.; Matli, P.R.; Shakoore, R.A.; Parande, G.; Manakari, V.; Mohamed, A.M.A.; Gupta, M. Using B₄C nanoparticles to enhance thermal and mechanical response of aluminum. *Materials* **2017**, *10*, 621. [[CrossRef](#)] [[PubMed](#)]
12. Barta, C.A.; Sachs-Barrable, K.; Jia, J.; Thompson, K.H.; Wasan, K.M.; Orvig, C. Lanthanide containing compounds for therapeutic care in bone resorption disorders. *Dalton Trans.* **2007**, 5019–5030. [[CrossRef](#)] [[PubMed](#)]
13. Bayani, H.; Saebnoori, E. Effect of rare earth elements addition on thermal fatigue behaviors of AZ91 magnesium alloy. *J. Rare Earths* **2009**, *27*, 255–258. [[CrossRef](#)]
14. Haque, N.; Hughes, A.; Lim, S.; Vernon, C. Rare earth elements: Overview of mining, mineralogy, uses, sustainability and environmental impact. *Resources* **2014**, *3*, 614–635. [[CrossRef](#)]
15. Kang, Y.-B.; Jin, L.; Chartrand, P.; Gheribi, A.E.; Bai, K.; Wu, P. Thermodynamic evaluations and optimizations of binary mg-light rare earth (La, Ce, Pr, Nd, Sm) systems. *Calphad* **2012**, *38*, 100–116. [[CrossRef](#)]
16. Tekumalla, S.; Gupta, M. An insight into ignition factors and mechanisms of magnesium based materials: A review. *Mater. Des.* **2017**, *113*, 84–98. [[CrossRef](#)]
17. Walker, J.; Shadanbaz, S.; Woodfield, T.B.; Staiger, M.P.; Dias, G.J. Magnesium biomaterials for orthopedic application: A review from a biological perspective. *J. Biomed. Mater. Res. Part B Appl. Biomater.* **2014**, *102*, 1316–1331. [[CrossRef](#)] [[PubMed](#)]
18. Cockeram, B. The fracture toughness and toughening mechanism of commercially available unalloyed molybdenum and oxide dispersion strengthened molybdenum with an equiaxed, large grain structure. *Metall. Mater. Trans. A* **2009**, *40*, 2843–2860. [[CrossRef](#)]
19. Liu, G.; Zhang, G.; Jiang, F.; Ding, X.; Sun, Y.; Sun, J.; Ma, E. Nanostructured high-strength molybdenum alloys with unprecedented tensile ductility. *Nat. Mater.* **2013**, *12*, 344–350. [[CrossRef](#)] [[PubMed](#)]
20. Kirkland, N.T. Magnesium biomaterials: Past, present and future. *Corros. Eng. Sci. Technol.* **2012**, *47*, 322–328. [[CrossRef](#)]
21. Navrotsky, A.; Lee, W.; Mielewczyk-Gryn, A.; Ushakov, S.V.; Anderko, A.; Wu, H.; Riman, R.E. Thermodynamics of solid phases containing rare earth oxides. *J. Chem. Thermodyn.* **2015**, *88*, 126–141. [[CrossRef](#)]
22. Martienssen, W.; Warlimont, H. Springer handbook of condensed matter and materials data. Springer Science & Business Media: Berlin, Germany, 2006.
23. Muneer, I.; Farrukh, M.A.; Javaid, S.; Shahid, M.; Khaleeq-ur-Rahman, M. Synthesis of Gd₂O₃/Sm₂O₃ nanocomposite via sonication and hydrothermal methods and its optical properties. *Superlattices Microstruct.* **2015**, *77*, 256–266. [[CrossRef](#)]
24. Herath, H.; Di Silvio, L.; Evans, J. In vitro evaluation of samarium (III) oxide as a bone substituting material. *J. Biomed. Mater. Res. Part A* **2010**, *94*, 130–136. [[CrossRef](#)] [[PubMed](#)]
25. Marker, T. *Development of a Laboratory-Scale Flammability Test for Magnesium Alloys Used in Aircraft Seat Construction*; Federal Aviation Administration William J. Hughes Technical Center: Egg Harbor Township, NJ, USA, 2014.
26. Parande, G.; Manakari, V.; Meenashisundaram, G.K.; Gupta, M. Enhancing the tensile and ignition response of monolithic magnesium by reinforcing with silica nanoparticulates. *J. Mater. Res.* **2017**, *32*, 1–10. [[CrossRef](#)]
27. Reddy, M.P.; Ubaid, F.; Shakoore, R.; Parande, G.; Manakari, V.; Mohamed, A.; Gupta, M. Effect of reinforcement concentration on the properties of hot extruded Al-Al₂O₃ composites synthesized through microwave sintering process. *Mater. Sci. Eng. A* **2017**, *696*, 60–69. [[CrossRef](#)]

28. Fida Hassan, S.; Al-Aqeeli, N.; Gasem, Z.; Tun, K.; Gupta, M. Magnesium nanocomposite: Increasing copperisation effect on high temperature tensile properties. *Powder Metall.* **2016**, *59*, 66–72. [[CrossRef](#)]
29. Vaidya, R.U.; Chawla, K. Thermal expansion of metal-matrix composites. *Compos. Sci. Technol.* **1994**, *50*, 13–22. [[CrossRef](#)]
30. Czerwinski, F. Overcoming barriers of magnesium ignition and flammability. *Adv. Mater. Process.* **2014**, *172*, 28–31.
31. Schwartz, M. *Encyclopedia and Handbook of Materials, Parts and Finishes*; Crc Press: Boca Raton, FL, USA, 2016.
32. Phillips, W. Oxidation of several lanthanide elements. *J. Less Common Met.* **1964**, *7*, 139–143. [[CrossRef](#)]
33. Nguyen, Q.; Gupta, M. Microstructure and mechanical characteristics of AZ31B/Al₂O₃ nanocomposite with addition of Ca. *J. Compos. Mater.* **2009**, *43*, 5–17. [[CrossRef](#)]
34. Manakari, V.; Parande, G.; Doddamani, M.; Gupta, M. Enhancing the ignition, hardness and compressive response of magnesium by reinforcing with hollow glass microballoons. *Materials* **2017**, *10*, 997. [[CrossRef](#)] [[PubMed](#)]
35. Parande, G.; Manakari, V.; Meenashisundaram, G.K.; Gupta, M. Enhancing the hardness/compression/damping response of magnesium by reinforcing with biocompatible silica nanoparticulates. *Int. J. Mater. Res.* **2016**, *107*, 1091–1099. [[CrossRef](#)]
36. Nguyen, Q.; Gupta, M. Enhancing compressive response of AZ31B magnesium alloy using alumina nanoparticulates. *Compos. Sci. Technol.* **2008**, *68*, 2185–2192. [[CrossRef](#)]
37. Hassan, S.; Gupta, M. Development of high strength magnesium copper based hybrid composites with enhanced tensile properties. *Mater. Sci. Technol.* **2003**, *19*, 253–259. [[CrossRef](#)]
38. Zhang, D.; Jiang, L.; Zheng, B.; Schoenung, J.; Mahajan, S.; Lavernia, E.; Beyerlein, I. Deformation twinning (update). *Ref. Modul. Mater. Sci. Eng.* **2015**, 1–24. Available online: <https://doi.org/10.1016/B978-0-12-803581-8.02878-2> (accessed on 31 October 2016).
39. Zhang, D.; Wen, H.; Kumar, M.A.; Chen, F.; Zhang, L.; Beyerlein, I.J.; Schoenung, J.M.; Mahajan, S.; Lavernia, E.J. Yield symmetry and reduced strength differential in Mg-2.5 Y alloy. *Acta Mater.* **2016**, *120*, 75–85. [[CrossRef](#)]
40. Stanford, N.; Barnett, M. The origin of “rare earth” texture development in extruded Mg-based alloys and its effect on tensile ductility. *Mater. Sci. Eng. A* **2008**, *496*, 399–408. [[CrossRef](#)]
41. Chen, Y.; Tekumalla, S.; Guo, Y.; Gupta, M. Introducing Mg-4Zn-3Gd-1Ca/ZnO nanocomposite with compressive strengths matching/exceeding that of mild steel. *Sci. Rep.* **2016**, *6*. [[CrossRef](#)] [[PubMed](#)]
42. Kumar, A.; Meenashisundaram, G.K.; Manakari, V.; Parande, G.; Gupta, M. Lanthanum effect on improving cte, damping, hardness and tensile response of Mg-3Al alloy. *J. Alloy. Compd.* **2017**, *695*, 3612–3620. [[CrossRef](#)]
43. Stecura, S.; Campbell, W.J. *Thermal Expansion and Phase Inversion of Rare-Earth Oxides*; US Dept. of the Interior, Bureau of Mines: Washington, DC, USA, 1961; Volume 5847.
44. Carreno-Morelli, E.; Urreta, S.; Schaller, R. Mechanical spectroscopy of thermal stress relaxation at metal–ceramic interfaces in aluminium-based composites. *Acta Mater.* **2000**, *48*, 4725–4733. [[CrossRef](#)]
45. Yi, H.-K.; Liu, Z.-T.; Li, F.-H. Investigation on room temperature damping vs strain amplitude behaviors of hypereutectic Al-17Si-xLa alloys. *J. Funct. Mater.* **2003**, *34*, 525–527.
46. Anilchandra, A.; Surappa, M. Microstructure and damping behaviour of consolidated magnesium chips. *Mater. Sci. Eng. A* **2012**, *542*, 94–103. [[CrossRef](#)]
47. Srikanth, N.; Zhong, X.; Gupta, M. Enhancing damping of pure magnesium using nano-size alumina particulates. *Mater. Lett.* **2005**, *59*, 3851–3855. [[CrossRef](#)]
48. Xiuqing, Z.; Haowei, W.; Lihua, L.; Naiheng, M. In situ synthesis method and damping characterization of magnesium matrix composites. *Compos. Sci. Technol.* **2007**, *67*, 720–727. [[CrossRef](#)]
49. Chung, D. Review: Materials for vibration damping. *J. Mater. Sci.* **2001**, *36*, 5733–5737. [[CrossRef](#)]
50. Zhang, J.; Gungor, M.; Lavernia, E. The effect of porosity on the microstructural damping response of 6061 aluminium alloy. *J. Mater. Sci.* **1993**, *28*, 1515–1524. [[CrossRef](#)]
51. Tsai, M.-H.; Chen, M.-S.; Lin, L.-H.; Lin, M.-H.; Wu, C.-Z.; Ou, K.-L.; Yu, C.-H. Effect of heat treatment on the microstructures and damping properties of biomedical Mg–Zr alloy. *J. Alloy. Compd.* **2011**, *509*, 813–819. [[CrossRef](#)]
52. Mallick, K. *Bone Substitute Biomaterials*; Elsevier: Amsterdam, The Netherlands, 2014.
53. Xu, T.; Zhang, N.; Nichols, H.L.; Shi, D.; Wen, X. Modification of nanostructured materials for biomedical applications. *Mater. Sci. Eng. C* **2007**, *27*, 579–594. [[CrossRef](#)]

54. Cho, K.; Niinomi, M.; Nakai, M.; Liu, H.; Santos, P.F.; Itoh, Y.; Ikeda, M. *Tensile and Compressive Properties of Low-Cost High-Strength β -Type Ti-Mn Alloys Fabricated by Metal Injection Molding*; Wiley Online Library: San Diego, CA, USA, 2015; pp. 499–503.
55. Henry, D. *Materials and Coatings for Medical Devices: Cardiovascular*; ASM International: Geauga County, OH, USA, 2009; pp. 151–186.
56. Handbook, M. *Properties and Selection: Nonferrous Alloys and Special-Purpose Materials*; ASM International: Geauga County, OH, USA, 1990; Volume 2, p. 102.
57. Puleo, D.A.; Huh, W.W. Acute toxicity of metal ions in cultures of osteogenic cells derived from bone marrow stromal cells. *J. Appl. Biomater.* **1995**, *6*, 109–116. [[CrossRef](#)] [[PubMed](#)]



© 2017 by the authors. Licensee MDPI, Basel, Switzerland. This article is an open access article distributed under the terms and conditions of the Creative Commons Attribution (CC BY) license (<http://creativecommons.org/licenses/by/4.0/>).